




Performance of optimal linear-response processes in driven Brownian motion far from equilibriumLucas P. Kamizaki ^{1,2,*}, Marcus V. S. Bonança ^{1,†} and Sérgio R. Muniz ^{2,‡}¹*Instituto de Física ‘Gleb Wataghin’, Universidade Estadual de Campinas, 13083-859 Campinas, São Paulo, Brazil*²*Instituto de Física de São Carlos, Universidade de São Paulo, 13560-970 São Carlos, São Paulo, Brazil*

(Received 14 June 2022; revised 17 October 2022; accepted 22 November 2022; published 19 December 2022)

Considering the paradigmatic driven Brownian motion, we perform extensive numerical analysis on the performance of optimal linear-response processes far from equilibrium. We focus on the overdamped regime where exact optimal processes are known analytically and most experiments operate. This allows us to compare the optimal processes obtained in linear response and address their relevance to experiments using realistic parameter values from experiments with optical tweezers. Our results help assess the accuracy of perturbative methods in calculating the irreversible work for cases where the exact solution might be difficult to access. For that, we present a performance metric comparing the approximate optimal solution to the exact one. Our main result is that optimal linear-response processes can perform surprisingly well, even far from where they were expected.

DOI: [10.1103/PhysRevE.106.064123](https://doi.org/10.1103/PhysRevE.106.064123)**I. INTRODUCTION**

Finite-time thermodynamic processes are ubiquitous. They are the way we control real-world systems and their environments [1–5]. However, the second law of thermodynamics states that nonequilibrium processes have an unavoidably higher cost than their quasistatic counterparts. Therefore, a major goal in science and engineering is understanding and searching for the minimal waste of resources to achieve a predetermined task. This leads to the fundamental problem of efficiency: finding the finite-time process with the minimum possible cost [6].

Taken in its full generality, the problem of finding optimal finite-time processes is a tough one, with few examples where exact solutions are known. A paradigmatic case where such solutions exist is the driven Brownian motion [7,8]. Its relevance is manifested by the number of experiments to test several different nonequilibrium phenomena. Using colloidal particles or beads trapped by optical tweezers, driven Brownian motion has been used to address fluctuation theorems [9–11], heat engines [12–14], feedback processes [15], Maxwell’s demons [16], and Landauer’s principle [17–19].

It seems natural to expect that the general features of the physics of optimal finite-time processes in driven Brownian systems might shed light on more complicated systems. As mentioned, exact analytical expressions for optimal processes are known in this case [7,8]. However, they present unexpected features such as jumps and sharp peaks that have been partially understood physically [20] and represent a real challenge for experimental implementation. Such counter-intuitive characteristics have been reproduced by numerical approaches based on optimal control [21–23], proving to be robust features [24,25]. However, this has not clarified the role of unexpected jumps and peaks in the optimal processes.

At the same time, perturbative approaches have been developed to provide approximate optimal finite-time protocols. They express the energetic cost of a given finite-time process in terms of functionals of the corresponding protocol, which are specific for certain regimes. If, on the one hand, these formulations restrict the optimization problem to limited nonequilibrium regimes, on the other hand, they provide a better physical intuition about the energetic cost through the quantities appearing in the derived functionals. Among these perturbative formulations, the so-called geometric approach has attracted considerable attention in the last decade [26–41]. It has been applied to different nonequilibrium situations in biophysics [34,36,39], magnetic systems [32,33,38], heat engines [37,42], and solid-state physics [43]. It also has been extended to quantum systems [30,35]. In this approach, the energetic cost is written as the time integral of a Lagrangian, understood as a thermodynamic metric [44–46]. The optimal finite-time processes, then, have the interpretation of being the corresponding geodesics.

Here, we show that the perturbative approach derived in Ref. [47] performs quite well beyond its expected range of validity, while the performance of the geometric approach, despite its relevance, is generally worse in the far from equilibrium region. Taking driven Brownian motion in the overdamped regime as a benchmark, we compare the performance of exact and approximate optimal protocols obtained from either Ref. [47] or the geometric approach and present it using realistic numbers, motivated by current experiments. Our extensive numerical analysis shows a clear advantage of the perturbative formulation in describing the optimal energetic cost far from equilibrium within a range of experimentally relevant values of the parameters involved. Additionally, the optimal protocols of Ref. [47] clearly consist of continuous and smooth versions of the exact optimal protocols derived in Ref. [7]. Therefore, in addition to being very attractive for experimental implementations, these approximate optimal protocols show that even smooth but fast changes at the right places of the process consist of a good (but

*kamizaki@ifi.unicamp.br

†mbonanca@ifi.unicamp.br

‡srmuniz@ifsc.usp.br

unexpected) optimization strategy far from equilibrium. This fact supports the claim that the perturbative approaches, in contrast to optimal control numerical methods, can potentially increase our physical understanding of optimal nonequilibrium processes.

We try to keep the presentation self-contained, so the manuscript is organized as follows. In Secs. II and III, we establish notations reviewing the standard theoretical description of Brownian motion and its corresponding stochastic thermodynamics, respectively. In Sec. IV, we rederive the exact optimal protocols [7] for driven Brownian motion in the overdamped regime and define the performance metric that we test numerically. In Sec. V, we present the basic elements of the geometric approach applied to driven Brownian motion and derive the corresponding optimal protocols, which we use later in our performance analysis. In Sec. VI, we obtain fast but weak optimal processes using the approach of Ref. [47] and obtain their performance far from equilibrium. Finally, we give our final remarks in Secs. VII and VIII.

II. DESCRIPTION OF BROWNIAN MOTION

A. Langevin equation

If $x(t)$ is the position at time t of a small particle of mass m subjected to a potential $V(x)$ and immersed in a liquid with friction coefficient γ at temperature T , the equation describing the particle's motion is given by

$$m \frac{d^2 x(t)}{dt^2} = -\frac{d}{dx} V[x, \lambda(t)] - \gamma \frac{dx(t)}{dt} + \sqrt{2k_B T \gamma} \xi(t), \quad (1)$$

which is known as the Langevin equation. We denote by $\lambda(t)$ a possible time dependence through a control parameter. The last term on the right-hand side, $\xi(t)$, is the stochastic term. It describes a stochastic force modeled as a random Gaussian white noise with zero mean. Mathematically, this corresponds to

$$\overline{\xi(t)} = 0 \quad (2)$$

and

$$\overline{\xi(t)\xi(t')} = \delta(t - t'). \quad (3)$$

The overbar denotes averages under different realizations of the white noise.

B. Simulations: Setup and realistic parameters

Optical tweezers are versatile tools used to trap and manipulate microscopic particles [48–50], from single atoms to macromolecules like DNA/RNA, up to living cells, and a wide range of colloidal particles [4,10,12,13].

Motivated by current experiments using optical trapping and dynamical control to test and explore ideas of nonequilibrium thermodynamics [51–53], we performed numerical simulations of a trapped spherical colloidal particle immersed in water at room temperature, using standard numerical tools [54].

For sufficiently large colloidal particles (typically with a radius r in the micrometer range) near the focus of a Gaussian laser beam, the confining optical potential near the focus can

TABLE I. Parameters used in the numerical simulations. These are typical values in optical tweezers experiments with colloidal particles [49].

Physical quantity	Representation	Value
Particle's radius	r	1 μm
Particle's density	ρ	2.65 g/cm ³
Particle's mass	m	11 pg
Friction coefficient	γ	1.89 $\times 10^{-8}$ Ns/m
Medium's temperature	T	300 K
Initial trap stiffness	κ	1 pN/ μm

be safely approximated by a simple harmonic potential,

$$V(x, \kappa) = \frac{\kappa(x - x_c)^2}{2}, \quad (4)$$

where κ represents the trapping (stiffness) constant, and x_c is the position of the trap center. The values of the other relevant parameters in Eq. (1) are shown explicitly in Table I. These are realistic values commonly used in experimental setups, and the main results of this present work are obtained using these values, except where it is mentioned otherwise.

We stress that the values of parameters listed in Table I lead to overdamped Brownian motion. This is an important point since the exact optimal protocols we will consider in Sec. IV are obtained in this regime and will be used as our benchmark. Nevertheless, our numerical simulations are performed using Eq. (1), which includes the inertia term. This choice is justified because inertia is indeed always present in experiments, and it may play a role even in the overdamped regime when the processes become fast enough, as those considered in Sec. VI.

III. STOCHASTIC THERMODYNAMICS OF DRIVEN BROWNIAN MOTION

In the late 1990s, Sekimoto [55] showed that work and heat can be associated with individual trajectories of a Brownian particle. In our case, by varying the stiffness parameter κ or the center position x_c in time, the expression of the average work performed during the process is

$$\langle W \rangle = \int_0^\tau dt \frac{d\lambda(t)}{dt} \left\langle \frac{\partial V(x, \lambda)}{\partial \lambda} \right\rangle, \quad (5)$$

where $\lambda(t)$ denotes a control parameter varied according to a protocol of duration τ . The symbol $\langle \cdot \rangle$ denotes an average over many microscopic realizations with initial conditions sampled from an equilibrium distribution.

In the previous expression for $\langle W \rangle$, the potential V could be substituted by the Hamiltonian H of the system, and the protocol $\lambda(t)$ could be rewritten as

$$\lambda(t) = \lambda_i + (\lambda_f - \lambda_i)g(s), \quad (6)$$

where $s = t/\tau$ and $g(s)$ describes the time change of $\lambda(t)$ with boundary conditions: $g(0) = 0$, and $g(1) = 1$.

Here, we focus on the harmonic potential with time-dependent stiffness, $\lambda(t) = \kappa(t)$. Considering $x_c = 0$, we have

the following time-dependent potential:

$$V[x, \lambda(t)] = \frac{\lambda(t)x^2}{2}. \quad (7)$$

The values chosen for $\lambda_{i,f}$, corresponding to the initial and final values, are motivated by the experimental implementation in optical tweezers. For values too small, the particle may escape the detection region during the experiment, while for values too large, the variation of the particle's position may become difficult to detect.

We emphasize that we will restrict ourselves to processes in which the particle starts in equilibrium, and the initial and final values of λ together with the duration τ of the protocol are the only boundary conditions. This contrasts with other works in the literature (see, for instance, Refs. [25,56]) in which a final equilibrium state is given as a boundary condition. Hence, in this study, the system *is not* in thermal equilibrium at the end of the considered protocols. However, the relaxation that happens afterwards, keeping λ fixed at λ_f , *does not* change the work performed since only heat is exchanged at this point. Thus, our optimization problem seeks an answer to the following problem: how to spend the minimal amount of energy along a finite-time variation of λ from λ_i to λ_f in a time interval τ given that the system of interest is initially in equilibrium with $\lambda = \lambda_i$. We remark that these are the boundary conditions often used in experiments such as those in Refs. [12,57].

Considering the time-independent version of potential (7), the Langevin equation, Eq. (1) can be solved to determine the dependence of the average values with time [58,59]. For a given out-of-equilibrium initial condition, the averages have a characteristic time scale that roughly measures the relaxation time τ_R to the thermal equilibrium values. A careful analysis shows that the relaxation time is $\tau_R = \gamma/(2\kappa)$ (see Sec. V for the details) and using the values in Table I, we find that it is equal to 9.4 ms for $\kappa = 1.0$ pN/ μm . This natural time scale allows the classification of the protocols into slow or fast. Given an initial trap stiffness, protocols with $\tau \ll \tau_R$ drive the system to regions far from equilibrium and are considered fast, while for protocols with $\tau \gg \tau_R$ the system remains close to equilibrium throughout the process and are considered slow.

As the process approaches the quasistatic limit, the average work tends to the Helmholtz free-energy difference ΔF between the final and initial equilibrium states, in agreement with the Kelvin-Planck statement of the second law of thermodynamics [60],

$$\langle W \rangle - \Delta F \equiv \langle W_{\text{irr}} \rangle \geq 0, \quad (8)$$

where $\langle W_{\text{irr}} \rangle$ is the average excess (irreversible) work paid in a finite-time process.

The expression for $F(\lambda)$ can be obtained using statistical mechanics, and it is given by

$$\begin{aligned} F(\lambda) &= -k_B T \ln Z \\ &= -k_B T \ln \int \exp[-H(\Gamma, \lambda)/k_B T] d\Gamma, \end{aligned} \quad (9)$$

where

$$Z = \int \exp[-H(\Gamma, \lambda)/k_B T] d\Gamma \quad (10)$$

is the partition function, $H(\Gamma, \lambda) = p^2/2m + V(x, \lambda)$ denotes the Hamiltonian of the Brownian particle (which includes kinetic energy due to what was explained in Sec. II), and Γ represents a point (x, p) in phase space. For the harmonic potential with time-dependent stiffness, the free-energy difference reads

$$\Delta F(\lambda) = k_B T \ln \left(\sqrt{\frac{\lambda_f}{\lambda_i}} \right), \quad (11)$$

where we used Eqs. (4) and (9), and λ_i and λ_f are the initial and final values of the stiffness parameter, respectively, as stated before.

We stress that the particle is out of equilibrium at the end of the protocols considered here. Thus, the free-energy difference just presented refers to the final equilibrium state that the particle will attain after equilibration at the end of the protocol.

IV. EXACT OPTIMAL PROTOCOLS IN THE OVERDAMPED REGIME

In some cases, it is possible to derive exact expressions for the optimal protocols performed in driven overdamped Brownian motion. In this section, we review the main steps of the derivation [7] since they will be our benchmark for analyzing the performance of optimal linear-response processes. Therefore, following Ref. [7] and restricting ourselves to the change in the stiffness parameter, Eq. (5) becomes

$$\langle W \rangle = \frac{1}{2} \int_0^\tau dt \frac{d\lambda}{dt} \langle x^2 \rangle = \frac{1}{2} \int_0^\tau dt \frac{d\lambda}{dt} w(t), \quad (12)$$

where $w(t) = \langle x^2 \rangle$. The time evolution of $w(t)$ can be obtained multiplying the corresponding Fokker-Planck equation by x^2 and integrating over x [7]. This yields

$$\frac{dw}{dt} = -\frac{2\lambda}{\gamma} w + \frac{2k_B T}{\gamma}. \quad (13)$$

This differential equation can be solved given an initial condition $w(0)$. Integrating Eq. (12) by parts, we obtain

$$\langle W \rangle = \frac{1}{2} \left(\lambda(t) w(t) \Big|_0^\tau - \int_0^\tau \lambda \frac{dw(t)}{dt} dt \right). \quad (14)$$

Isolating λ in Eq. (13) and substituting the result in the previous expression, we rewrite Eq. (14) as

$$\langle W \rangle = \frac{1}{2} \left[w(t) \lambda(t) - k_B T \ln w(t) \right] \Big|_0^\tau + \frac{\gamma}{4} \int_0^\tau \frac{1}{w} \left(\frac{dw}{dt} \right)^2 dt. \quad (15)$$

To find the optimal protocol, one can first minimize the integral on the right-hand side. The minimization of this functional corresponds to solving the Euler-Lagrange equation

$$\left(\frac{dw}{dt} \right)^2 - 2w \frac{d^2 w}{dt^2} = 0, \quad (16)$$

whose solution is

$$w(t) = c_1 (1 + c_2 t)^2. \quad (17)$$

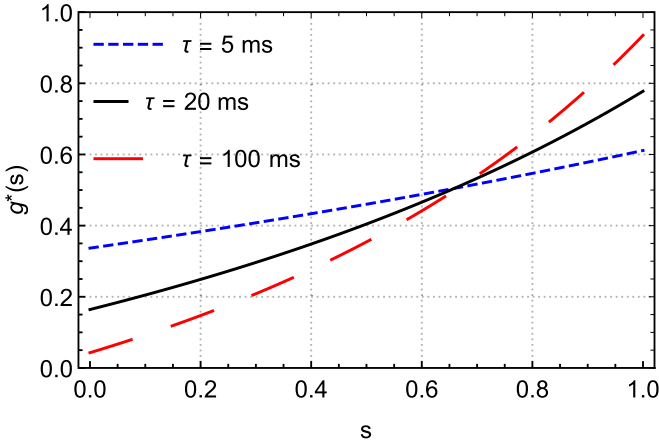


FIG. 1. Exact optimal protocol $\lambda^*(t)$ given by Eq. (20), and rewritten as $\lambda^*(s) = \lambda_i + \Delta\lambda g^*(s)$, as a function of $s = t/\tau$ for different values of τ . The initial and final values of λ were chosen as $\lambda_i = 1.0$ pN/ μm and $\lambda_f = 2.5$ pN/ μm , and $\Delta\lambda = \lambda_f - \lambda_i$. The faster the protocol is, the greater the initial and final jumps.

The c_1 and c_2 are constants to be determined. For instance, if initially the particle is in thermal equilibrium, then $w(0) = c_1 = k_B T / \lambda_i$. The other constant, c_2 , we find by minimizing the work in Eq. (14) after using Eq. (17) with $c_1 = k_B T / \lambda_i$,

$$\frac{\langle W \rangle}{k_B T} = \frac{\lambda_f}{2\lambda_i} (1 + \tau c_2)^2 + \frac{(\tau c_2)^2 \gamma}{\lambda_i \tau} - \frac{1}{2} - \ln(1 + c_2 \tau). \quad (18)$$

The value of c_2 that minimizes the previous expression is equal to

$$c_2 \tau = \frac{-\gamma - \tau \lambda_f + \sqrt{\gamma^2 + 2\gamma \tau \lambda_i + \tau^2 \lambda_f \lambda_i}}{2\gamma + \lambda_f \tau}. \quad (19)$$

Finally, using Eqs. (13), (17), and (19), we obtain the optimal protocol $\lambda^*(t)$ for the time-dependent stiffness,

$$\lambda^*(t) = \frac{\lambda_i - \gamma c_2 (1 + c_2 t)}{(1 + c_2 t)^2}. \quad (20)$$

We remark that, for $t = 0$, the expression above leads to

$$\lambda^*(0) = \lambda_i - \gamma c_2 \neq \lambda_i.$$

Thus, the optimal protocol $\lambda^*(t)$ has a discontinuity at the initial time $t = 0$. The same happens for $t = \tau$, i.e., $\lambda^*(\tau) \neq \lambda_f$. Figure 1 illustrates these discontinuities, showing that they decrease as the process becomes slower.

In addition, Fig. 1 shows that, for a fixed and not so small change $\Delta\lambda = \lambda_f - \lambda_i$ of the control parameter, larger values of τ lead to a more accentuated curvature of the exact optimal protocol. This implies that the rate of change $d\lambda^*/dt$ becomes stationary (apart from the jumps at the boundaries) as the process becomes faster. In other words, solution (20) contains the following physics: a time-dependent rate protocol is not a good optimization strategy if the protocol time τ becomes comparable with the relaxation time τ_R . This will be corroborated by the perturbative approaches discussed in Secs. V and VI.

We additionally remark that the Gaussian statistics in the harmonic confinement can be further explored as a complementary approach to the problem (see, for instance, Ref. [61]).

A. Limiting cases

As verification of expression (18), we can take the limits of arbitrarily short or long protocol duration. For extremely short protocols, we have

$$\lim_{\tau \rightarrow 0} c_2 \tau \rightarrow 0 \quad (21)$$

and

$$\frac{\langle W \rangle}{k_B T} \rightarrow \frac{1}{2} \left(\frac{\lambda_f}{\lambda_i} - 1 \right), \quad (22)$$

which is equal to the average work of the instantaneous protocol, leading to a variation $\Delta\lambda = \lambda_f - \lambda_i$, as expected. For arbitrarily long protocols,

$$\lim_{\tau \rightarrow \infty} c_2 \tau \rightarrow \left(\sqrt{\frac{\lambda_f}{\lambda_i}} - 1 \right) \quad (23)$$

and

$$\langle W \rangle \rightarrow \Delta F = k_B T \ln \left(\sqrt{\frac{\lambda_f}{\lambda_i}} \right). \quad (24)$$

So, the average work in the quasistatic limit is indeed equal to the free-energy difference.

B. Performance

Equations (18) and (19) give the minimum average work required to change $\lambda(t)$ from λ_i to λ_f in a finite-time process of fixed duration τ . In more complex cases, the work functional (5) may not be so easy to optimize, justifying the necessity of other optimization methods. To compare the perturbative approaches of Secs. V and VI with the analytical solution presented in this section, we define the performance \mathcal{P} as the relative difference between the average works $\langle W \rangle_{\text{approx}}$ and $\langle W \rangle_{\text{exact}}$ performed along the approximate and the exact optimal protocols, respectively, i.e.,

$$\mathcal{P} = \frac{\langle W \rangle_{\text{approx}} - \langle W \rangle_{\text{exact}}}{\langle W \rangle_{\text{exact}}}. \quad (25)$$

We say that a method has a good performance when the value of the relative difference \mathcal{P} is sufficiently small.

We take the chance to emphasize how the quantities $\langle W \rangle_{\text{exact}}$ and $\langle W \rangle_{\text{approx}}$ are calculated. $\langle W \rangle_{\text{exact}}$ is computed analytically from Eqs. (18) and (19). $\langle W \rangle_{\text{approx}}$ is obtained as the average over several realizations obtained from the numerical integration of Eq. (1) with a specific choice of $\lambda(t)$. In the case of $\langle W \rangle_{\text{exact}}$, $\lambda(t)$ is given by Eq. (20), and for $\langle W \rangle_{\text{approx}}$, it is taken from the perturbative descriptions of Secs. V and VI. This means that the work performed along each microscopic realization of $\lambda(t)$ is calculated in the standard way from the trajectories generated by Eq. (1), which has the inertia term. In other words, we stress that in our analyses of the performance we have never considered approximated expressions for the average work to compute $\langle W \rangle_{\text{approx}}$. Hence, the $\langle W \rangle_{\text{approx}}$ used in Eq. (25) is always obtained from averages of distributions of work values calculated from numerical simulations using Eq. (1).

We have also considered the performance coefficient

$$Q = \frac{\langle W_{\text{irr}} \rangle_{\text{approx}} - \langle W_{\text{irr}} \rangle_{\text{exact}}}{\langle W_{\text{irr}} \rangle_{\text{exact}}}, \quad (26)$$

which gives the relative difference of the *irreversible* contributions. According to Eq. (8), each quantity in the previous expression is obtained subtracting the free-energy difference ΔF [Eq. (11)] from its corresponding partner in Eq. (25).

V. OPTIMAL SLOWLY VARYING PROCESSES

The first perturbative approach we will discuss describes the work performed along slowly varying processes. It is based on linear response theory (LRT) and on the assumption that, for slow enough processes, the relaxation to equilibrium happens much faster than the variation of the control parameter. In other words, we will deal with near-equilibrium processes in the vicinity of quasistatic variations. Next, we reproduce the main steps of deriving the functional measuring the energetic cost for this class of processes. We will follow closely Refs. [26,28,43]. For an alternative derivation based on endoreversibility, see Ref. [62].

In the linear response regime ($\Delta\lambda/\lambda_i \ll 1$), we can expand the Hamiltonian of the system of interest as

$$H[\lambda(t)] = H(\lambda_i) + \Delta\lambda g(t)\partial_\lambda H + \mathcal{O}(\Delta\lambda^2), \quad (27)$$

where we used Eq. (6) to express $\lambda(t)$ in terms of $g(t)$. Then, by using the well-known methods of LRT [63], we obtain the nonequilibrium average of the generalized force $\partial_\lambda H \equiv \partial H/\partial\lambda$,

$$\begin{aligned} \langle \partial_\lambda H(t) \rangle &= \langle \partial_\lambda H(0) \rangle_{\text{eq};\lambda_i} + \chi_0^\infty \Delta\lambda g(t) \\ &\quad - \Delta\lambda \int_0^t ds \phi(t-s)g(s), \end{aligned} \quad (28)$$

where $\langle \cdot \rangle_{\text{eq};\lambda_i}$ is the average over the equilibrium canonical distribution, $\exp[-H(\Gamma, \lambda)/k_B T]/Z$, with control parameter $\lambda = \lambda_i$. The second term on the right-hand side describes the instantaneous response,

$$\chi_0^\infty = \left\langle \frac{\partial^2 H}{\partial \lambda^2} \right\rangle_{\text{eq};\lambda_i}, \quad (29)$$

while the last term is the delayed response. The function $\phi(t)$ is the response function [63],

$$\phi(t) = \langle \{ \partial_\lambda H(0), \partial_\lambda H(t) \} \rangle_{;\lambda_i} \quad (30)$$

where $\{ \cdot, \cdot \}$ is the Poisson bracket. Employing Kubo's formula, we find the relaxation function $\Psi(t)$,

$$\Psi(t) = \beta \left(\langle \partial_\lambda H(0) \partial_\lambda H(t) \rangle_{\text{eq};\lambda_i} - \langle \partial_\lambda H(0) \rangle_{\text{eq};\lambda_i}^2 \right), \quad (31)$$

where $\phi(t) = -d\Psi(t)/dt$ and $\beta = (k_B T)^{-1}$. Therefore, Eq. (28) can be rewritten after an integration by parts as

$$\begin{aligned} \langle \partial_\lambda H(t) \rangle &= \langle \partial_\lambda H(0) \rangle_{\text{eq};\lambda_i} - \tilde{\Psi} \Delta\lambda g(t) \\ &\quad + \Delta\lambda \int_0^t du \Psi(u) \frac{dg}{dt} \Big|_{t'=t-u}, \end{aligned} \quad (32)$$

where $\tilde{\Psi} = \Psi(0) - \chi_0^\infty$.

Considering that $\Psi(t)$ decays sufficiently fast to assume dg/dt is approximately constant within this time scale, the convolution in the right-hand side of the previous expression

can be written as [26,28]

$$\begin{aligned} \int_0^t du \Psi(u) \frac{dg}{dt} \Big|_{t'=t-u} &\approx \frac{dg}{dt} \int_0^t du \Psi(u) \\ &\approx \frac{dg}{dt} \int_0^\infty du \Psi(u), \end{aligned} \quad (33)$$

where we have further assumed that extending the upper limit to infinity does not change the result significantly [this is probably justified only in cases where $\Psi(t)$ decays exponentially].

Applying Eq. (32) and approximation (33) to each infinitesimal variation of λ along the protocol $\lambda(t)$, and plugging them into Eq. (5) to compute the work performed, one finally finds the functional (see Refs. [26,28] for more details)

$$\begin{aligned} \langle W_{\text{irr}} \rangle &= \langle W \rangle - \Delta F \\ &= \frac{\beta(\Delta\lambda)^2}{\tau} \int_0^1 ds \left(\frac{dg}{ds} \right)^2 \tau_R[g(s)] \chi[g(s)] \end{aligned} \quad (34)$$

for the so-called irreversible work $\langle W_{\text{irr}} \rangle$ [see Eq. (8)]. The quantities $\tau_R[g(s)]$ and $\chi[g(s)]$ represent the parametric change of the relaxation time,

$$\tau_R(\lambda) = \int_0^\infty \frac{\Psi(u)}{\Psi(0)} du, \quad (35)$$

and of the equilibrium fluctuations of the generalized force $\partial_\lambda H$,

$$\chi(\lambda) = \Psi(0)/\beta = \langle (\partial_\lambda H)^2 \rangle_{\text{eq};\lambda} - \langle \partial_\lambda H \rangle_{\text{eq};\lambda}^2, \quad (36)$$

along the protocol $\lambda(t)$. Due to the parametric change of λ , we write the averages in the previous expression for a generic value of λ .

Equation (34) provides the following physics: (i) it predicts a regime in which the energetic cost scales as τ^{-1} no matter the shape of the protocol, (ii) the protocol must be slowed down where the change of $\tau_R \cdot \chi$ [64] increases in order to minimize the cost, and (iii) the power related to the irreversible loss of energy resembles Joule heating [it is proportional to $(dg/dt)^2$], and it is constant along optimal protocols with single control parameters [26].

The $\lambda^*(t)$ that minimizes Eq. (34) can be found via standard methods of calculus of variations once τ_R and χ are known. For the example of driven Brownian motion, exact analytical expressions can be obtained using Eqs. (35) and (36) as we show next. For more complex situations, analytical approximations [28] or numerical methods can be used [65]. For instance, it is shown in Ref. [28] that the relaxation function can be obtained through a self-consistent phenomenological approach based on linear-response sum rules.

A. Relaxation function for the stiffening trap

For the harmonic potential with time-dependent stiffness, the generalized force is simply

$$\partial_\lambda H = \frac{x^2}{2}. \quad (37)$$

Then, according to Eq. (31), the relaxation function in this case reads

$$\Psi(t) = \frac{\beta}{4} \left(\langle (x(0)^2 x(t)^2) \rangle_{\text{eq};\lambda} - \langle x(0)^2 \rangle_{\text{eq};\lambda}^2 \right). \quad (38)$$

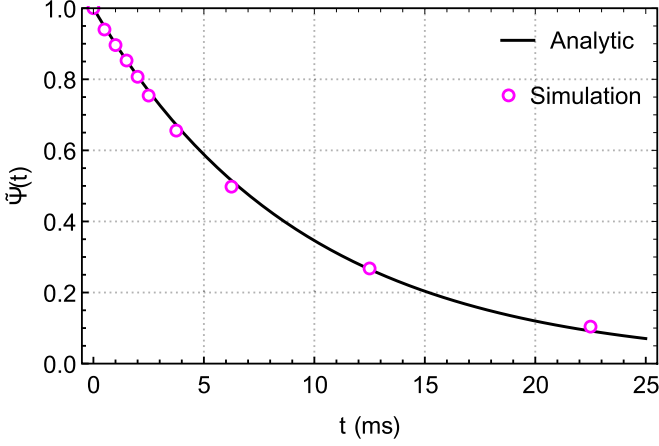


FIG. 2. Comparison between analytical [Eq. (39)] (black solid line) and numerical calculations (magenta dots) of $\tilde{\Psi}(t) = \Psi(t)/\Psi(0)$ [Eq. (38)] for the stiffening trap in the overdamped regime using the parameter values of Table I. Our numerical simulations integrate Eq. (1) and allow for the numerical calculation of the averages in Eq. (38). The result shows the complete absence of damped oscillations.

Hence, the relaxation function is found calculating the two-point equilibrium correlation of position squared. In other words, to obtain the relaxation function, we must measure/calculate the position $x(t)$ and obtain the correlation $\langle x(0)^2 x(t)^2 \rangle_{\text{eq};\lambda}$ and the average $\langle x(0)^2 \rangle_{\text{eq};\lambda}$ when the control parameter is kept fixed at the initial value.

To obtain an analytical expression, note that the trajectory of a particle in a harmonic potential can be found by solving the Langevin equation, Eq. (1). The average values can be found using the properties of the thermal noise given by Eqs. (2) and (3). Additionally, it is necessary to use the information that the system is initially in thermal equilibrium and that the initial conditions are distributed accordingly. Therefore, the relaxation function for the stiffening trap in the overdamped regime is equal to

$$\Psi(t) = \Psi(0) \left(\frac{s_2 e^{s_1 |t|} - s_1 e^{s_2 |t|}}{s_2 - s_1} \right)^2, \quad (39)$$

where

$$\Psi(0) = \frac{1}{2\beta\lambda^2}, \quad (40)$$

$$s_1 = \frac{-\gamma/m - \sqrt{(\gamma/m)^2 - 4(\lambda/m)}}{2}, \quad (41)$$

and

$$s_2 = \frac{-\gamma/m + \sqrt{(\gamma/m)^2 - 4(\lambda/m)}}{2}. \quad (42)$$

Figure 2 compares the analytical expression (39) with the relaxation function obtained from the numerical simulations of the Langevin equation, Eq. (1). It shows that expression (39) has a clear overdamped behavior, although it is written in terms of solutions of Eq. (1). This is due to the parameter values taken from Table I.

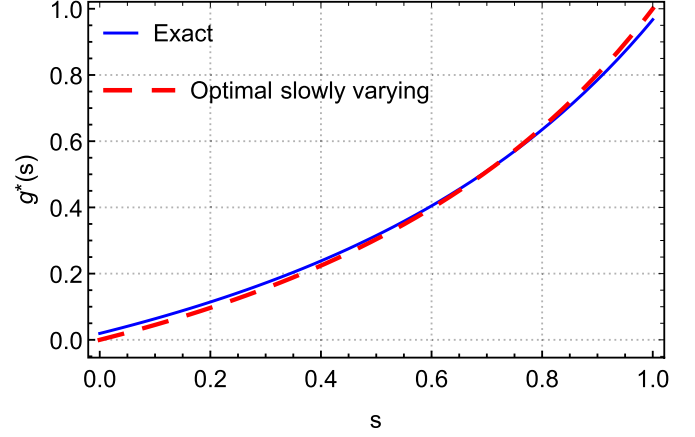


FIG. 3. Comparison between the exact optimal protocol (20) (blue solid line) and the optimal slowly varying protocol (46) (red dashed line) as a function of $s = t/\tau$. The relation between $\lambda(s)$ and $g(s)$ is given by Eq. (6). The parameters used are $\tau = 200$ ms, $\lambda_i = 1.0$ pN/ μm , $\lambda_f = 3.0$ pN/ μm , and $\tau_R(\lambda_i) = 9.4$ ms. The approximate optimal protocol (46) approaches the exact one as τ_R/τ decreases.

B. Optimal protocol for the stiffening trap

In order to obtain the optimal protocol for the stiffening trap, we first use Eqs. (39)–(42) in Eqs. (35) and (36) to obtain expressions for τ_R and χ . The latter reads

$$\chi(\lambda) = \frac{1}{4} \left(\langle x(0)^4 \rangle_{\text{eq};\lambda} - \langle x(0)^2 \rangle_{\text{eq};\lambda}^2 \right) = \frac{1}{2(\beta\lambda)^2}, \quad (43)$$

and the relaxation time is given by

$$\tau_R(\lambda) = \frac{\gamma}{2\lambda}, \quad (44)$$

when we consider the overdamped limit, i.e., after taking the limit $m \rightarrow 0$ in Eq. (39). Substituting the previous results in expression (34) for $\langle W_{\text{irr}} \rangle$, we obtain

$$\langle W_{\text{irr}} \rangle = \frac{\gamma(\Delta\lambda)^2}{4\beta\tau\lambda_i^3} \int_0^1 ds \left(\frac{dg}{ds} \right)^2 \frac{1}{\left[1 + \frac{\Delta\lambda}{\lambda_i} g(s) \right]^3}. \quad (45)$$

The minimum of this functional (after solving the Euler-Lagrange equation) is found for the protocol [28]

$$g^*(s) = -\frac{\lambda_i}{\Delta\lambda} + \frac{1}{A(s+B)^2}, \quad (46)$$

where A and B are given by the boundary conditions $g^*(0) = 0$ and $g^*(1) = 1$. The protocol (46) is depicted in Fig. 3, where we see how well it approximates the exact optimal protocol (20) for a small value of τ_R/τ .

The numerical analysis of the performance of this optimal protocol is part of our primary goal. This is shown in Fig. 4, where the coefficients \mathcal{P} [Eq. (25)] and \mathcal{Q} [Eq. (26)] are obtained for an extensive variation of the relative change $\Delta\lambda/\lambda_i$ of the control parameter and of the protocol duration τ . We remind that the work performed along the exact optimal protocol (20), denoted in Eq. (25) by $\langle W \rangle_{\text{exact}}$, is given by Eq. (18). The quantity $\langle W \rangle_{\text{approx}}$ used in \mathcal{P} (and \mathcal{Q}) is obtained from numerical simulations of Eq. (1) using a time-dependent stiffness parameter given by Eq. (46). The numerical average

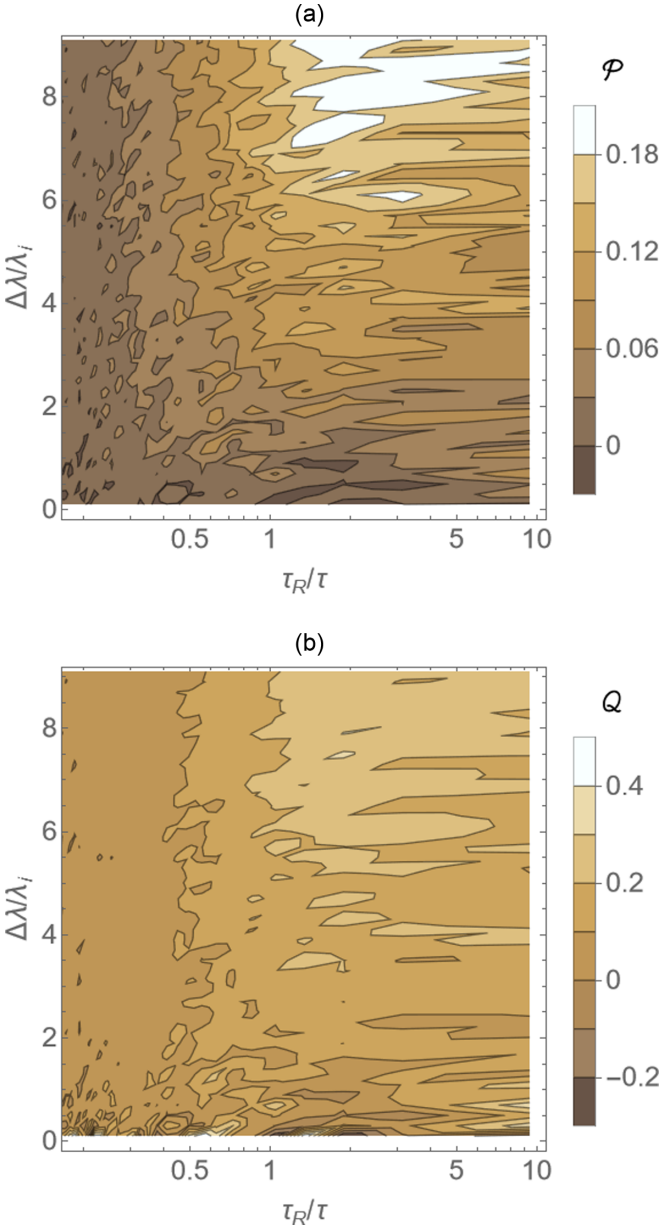


FIG. 4. Performance (a) \mathcal{P} (25) and (b) \mathcal{Q} (26) of the approximate optimal protocol (46) derived in Sec. V. We recall that $\langle W \rangle_{\text{exact}}$ (and $\langle W_{\text{irr}} \rangle_{\text{exact}} = \langle W \rangle_{\text{exact}} - \Delta F$) is obtained analytically using Eq. (18). The average work $\langle W \rangle_{\text{approx}}$ was obtained from 10^5 trajectories generated numerically using Eq. (1) with the approximate optimal protocol (46). We have set $\lambda_i = 1.0$ pN/ μm and $\tau_R(\lambda_i) = 9.4$ ms. The other parameters were chosen according to Table I.

leading to $\langle W \rangle_{\text{approx}}$ was obtained using 10^5 microscopic realizations.

As expected, the optimal protocol (46) performs better in the regime of slow processes, i.e., when $\tau_R/\tau < 1$. Increasing both $\Delta\lambda/\lambda_i$ and τ_R/τ , we enter the far-from-equilibrium region, and the performance of Eq. (46) decreases substantially. The irregular boundaries between regions with different values of \mathcal{P} are a consequence of our finite statistical sample. We remark that Fig. 4 does not check the range of validity of the functional (45). Instead, it tells us how well the optimal pro-

ocol obtained from this functional performs when compared with the protocol obtained from the exact solution (20).

VI. FAST BUT WEAK OPTIMAL PROCESSES

Linear response theory can also be used to describe a regime that is somewhat complementary to the one described previously. In other words, we will use LRT to describe a regime in which the protocols can be arbitrarily fast but restricted to small variations of the control parameter, i.e., $\Delta\lambda/\lambda_i < 1$. The functional for $\langle W_{\text{irr}} \rangle$ can be obtained in this case using, again, the nonequilibrium average (32) of the generalized force. However, we will keep the convolution in it, that is, we will not perform the approximation (33) since there will be no clear time-scale separation between the change in $\lambda(t)$ and the relaxation to equilibrium.

Reference [66] shows that plugging Eq. (32) into Eq. (5) leads to

$$\langle W_{\text{irr}} \rangle = \frac{(\Delta\lambda)^2}{2} \int_0^1 ds \int_0^1 ds' \Psi[\tau(s-s')] \frac{dg(s)}{ds} \frac{dg(s')}{ds'}, \quad (47)$$

where $s = t/\tau$, and $\Psi(t)$ is given again by Eq. (31). An effective strategy to minimize Eq. (47) is that described in Ref. [47]. It consists of expanding dg/ds in some basis of functions in the interval $s \in [0, 1]$. Due to its convenient mathematical properties, a good choice of basis is that formed by the Chebyshev polynomials $T_n(x)$ [67]. Following Refs. [47,67], the truncated and regularized expansion of dg/ds in a finite number N of polynomials $T_n(x)$ in the interval $[0, 1]$ then reads

$$\frac{dg(s)}{ds} = \sum_{n=1}^N a_n g_{N,n} T_n(2s-1), \quad (48)$$

where a_n are the coefficients to be determined and the factors $g_{N,n}$ regularize the truncated expansion [67] to avoid the Gibbs phenomenon at the extremities of the expansion interval. Their expression is [67]

$$g_{N,n} = \frac{N-n+1}{N+1} \cos\left(\frac{\pi n}{N+1}\right) + \frac{1}{N+1} \sin\left(\frac{\pi n}{N+1}\right) \cot\left(\frac{\pi}{N+1}\right). \quad (49)$$

Substituting expression (48) into Eq. (47), we obtain

$$\langle W_{\text{irr}} \rangle [(\Delta\lambda)^2 \Psi(0)/2]^{-1} = \sum_{n,l} A_{nl} a_n a_l, \quad (50)$$

where the A_{nl} are given by

$$A_{nl} = \int_0^1 \int_0^1 \tilde{\Psi}[\tau(s-s')] \times g_{N,n} g_{N,l} T_n(2s-1) T_l(2s'-1) ds' ds, \quad (51)$$

with $\tilde{\Psi}(t) = \Psi(t)/\Psi(0)$. The irreversible work in Eq. (47) becomes a finite multidimensional quadratic form whose minimum we want to find. The coefficients a_n that give such minimum value also have to obey the boundary conditions $g(0) = 0$ and $g(1) = 1$, which work as additional constraints

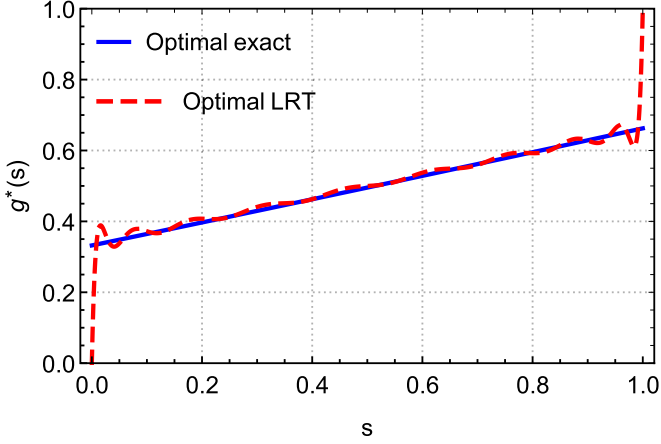


FIG. 5. Comparison between the exact optimal protocol (20) (blue solid line) and the protocol that minimizes Eq. (47) (red dashed line) as a function of $s = t/\tau$. The relation between $\lambda(s)$ and $g(s)$ is given by Eq. (6). These results refer to $N = 10$, $\lambda_i = 1.0$ pN/ μm , $\lambda_f = 1.1$ pN/ μm , $\tau = 9$ ms, and $\tau_R = 9.4$ ms. We used the relaxation function (39) with the parameter values in Table I.

in our optimization. Using the method of Lagrange multipliers, we can find the coefficients a_n that provide the optimal protocol by solving a set of linear algebraic equations.

We remark that the relaxation function $\Psi(t)$ is the main physical input to the optimization problem. The factors A_{nl} crucially depend on the protocol time τ and $\Psi(t)$. Due to its relation with the response function (30), $\Psi(t)$ can be obtained from experiments when it is not accessible theoretically. This is an advantage of this approximate method, which can be readily applied to general potentials for which one does not have an exact solution for the optimal protocol.

Figure 5 shows the optimal protocol obtained from minimizing Eq. (50) for specific values of τ and N . Although approaching the exact optimal solution (18) in most parts of the interval, the approximate optimal protocol clearly has smooth versions of the jumps presented by expression (18).

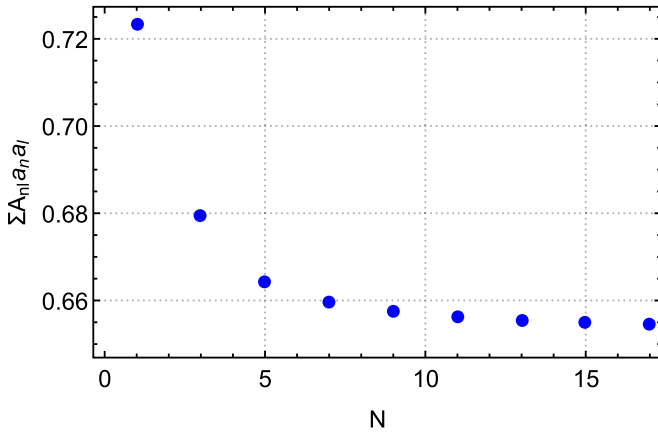


FIG. 6. Numerical evaluation of the right-hand side of Eq. (50), $\sum_{n,l} A_{nl} a_n a_l$, for different values of N , i.e., the number of polynomials used in Eq. (48). We used the coefficients a_n corresponding to the optimal protocol. The factors A_{nl} were calculated using expression (39) for $\Psi(t)$ and the parameter values in Table I. In particular, $\lambda_i = 1.0$ pN/ μm and $\tau = 9.0$ ms.

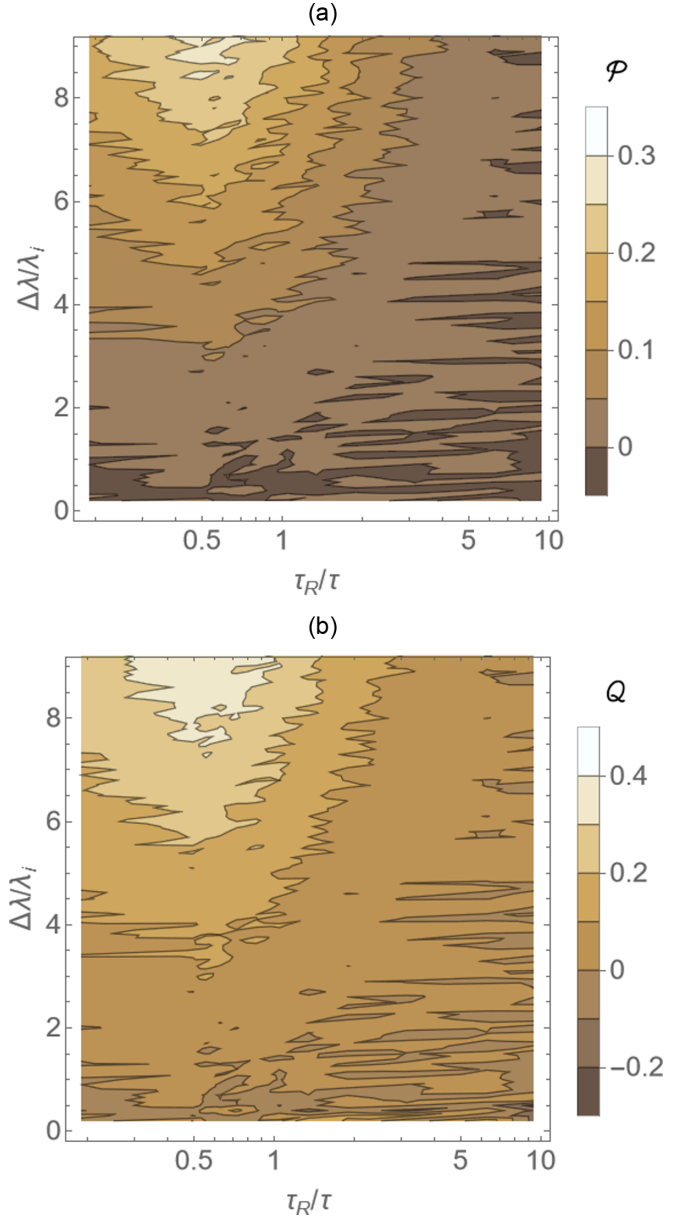


FIG. 7. Performance (a) \mathcal{P} [Eq. (25)] and (b) \mathcal{Q} [Eq. (26)] of the approximate optimal protocol derived in Sec. VI. We recall that $\langle W \rangle_{\text{exact}}$ (and $\langle W_{\text{irr}} \rangle_{\text{exact}} = \langle W \rangle_{\text{exact}} - \Delta F$) is obtained analytically using Eq. (18). The average work $\langle W \rangle_{\text{approx}}$ was obtained from 10^5 trajectories generated numerically using Eq. (1) with the approximate optimal protocol that minimizes the functional (47) (see the dashed line in Fig. 5). We have set $\lambda_i = 1.0$ pN/ μm and $\tau_R(\lambda_i) = 9.4$ ms. The other parameters were chosen according to Table I.

As shown in Ref. [47], such smooth jumps decrease as the value of τ increases and the process becomes slower, in agreement with the behavior of the exact solution (18). Reference [47] also shows that these smooth but steep features become sharper as the number of polynomials in Eq. (48) increases, providing a better agreement with the exact solution. However, Fig. 6 shows that the value of $\langle W_{\text{irr}} \rangle$ given by Eq. (47) does not change considerably for $N \gtrsim 10$. In other words, the optimization method just described is already efficient for low values of N .

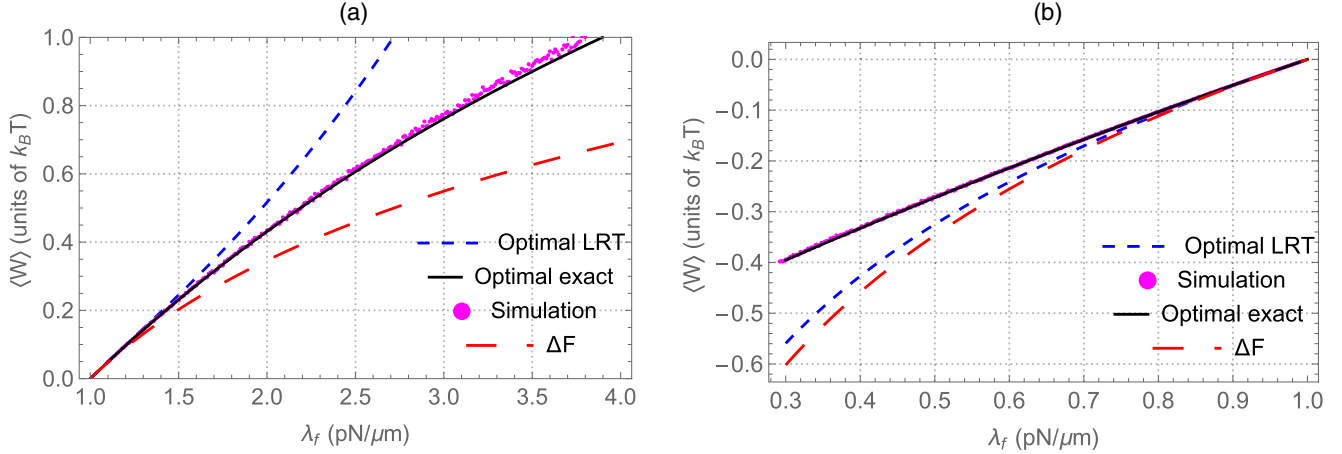


FIG. 8. Average work [Eq. (5)] as a function of λ_f for $\tau = 9.0$ ms and $\lambda_i = 1.0$ pN/ μm . The other parameters were chosen according to Table I. The protocol $\lambda(t)$ increases the stiffness in (a) and decreases it in (b). The black solid line shows Eq. (18). The blue dashed line shows Eq. (47) for its optimal protocol with $N = 10$. Using this protocol, we have simulated the Langevin dynamics, using Eq. (1), and obtained the average work shown in magenta dots using 10^4 trajectories. The good performance of the approximate optimal protocol goes beyond the range of validity of expression (47).

Figure 7 shows the performance coefficients \mathcal{P} [Eq. (25)] and \mathcal{Q} [Eq. (26)] of the approximate optimal protocols that minimize Eq. (47) for an extensive variation of the relative change $\Delta\lambda/\lambda_i$ of the control parameter, and of the protocol duration τ . Analogously to the results of Fig. 4, the work performed along the approximate optimal protocol was obtained from the numerical simulations of Eq. (1) using 10^5 trajectories. Again, the performance is excellent in the region of $\Delta\lambda/\lambda_i \ll 1$. Nevertheless, it remains very good in most of the far-from-equilibrium region. This is in clear contrast to the performance of optimal protocols obtained in Sec. V using the geometric approach.

The outstanding performance of the protocols minimizing Eq. (47) far from equilibrium is substantiated in Fig. 8. There, it is shown that when we drive the Brownian particle using the approximate optimal protocols, the work performed is almost indistinguishable from that using the exact optimal protocol

(18), even when $\Delta\lambda/\lambda_i > 1$. The validity of Eq. (47) is, however, restricted to a small range. Figures 8(a) and 8(b) depict, respectively, work values when the protocol $\lambda(t)$ increases and decreases the value of the stiffness parameter.

VII. EXCESS POWER

Figures 9–11 show the comparison between the exact excess power, i.e., the excess power along the exact optimal protocol (20), and that obtained from the approximate optimal protocols of Secs. V and VI. By excess power, we mean the quantity whose integral gives the irreversible work $\langle W_{\text{irr}} \rangle = \langle W \rangle - \Delta F$. For instance, Eq. (5) gives the total work as the integral of the total power. Thus, the excess power does not account for the power delivered to change the free energy.

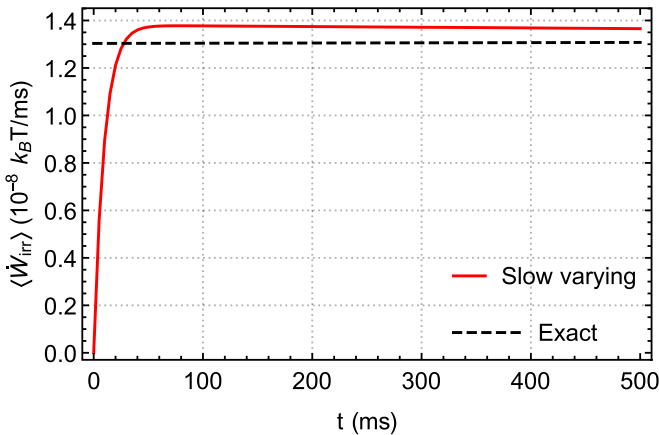


FIG. 9. Comparison between the excess power [Eq. (52)] along the exact optimal protocol (20) (black dashed line) and the optimal slowly varying protocol (46) (red solid line). The parameters are $\tau = 500$ ms, $\tau_R = 9.4$ ms, $\lambda_i = 1.0$ pN/ μm , and $\lambda_f = 3.0$ pN/ μm .

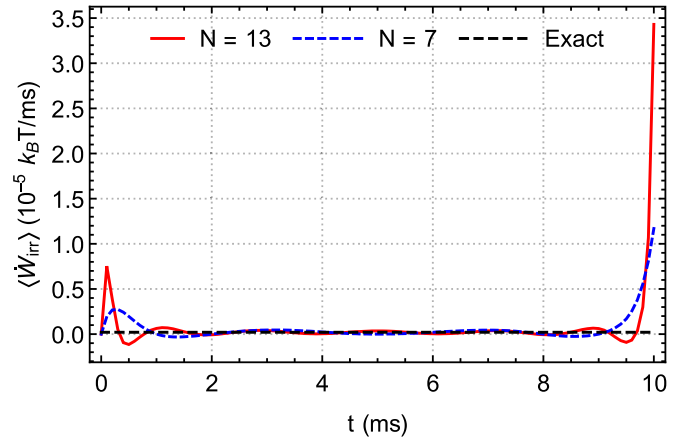


FIG. 10. Excess power [Eq. (52)] for different optimal protocols using parameters $\tau = 10$ ms, $\tau_R = 9.4$ ms, $\lambda_i = 1.0$ pN/ μm , and $\lambda_f = 1.2$ pN/ μm . The red solid line and the blue dashed line depict the excess power along the protocols minimizing Eq. (47) with $N = 13$ and $N = 7$, respectively. The black dashed line depicts the excess power along the exact optimal protocol (20).

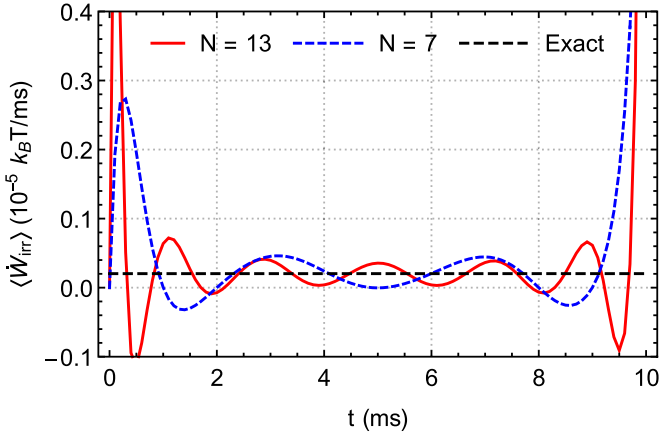


FIG. 11. Zoom-in of Fig. 10. The excess power [Eq. (52)] along the approximate optimal protocols of Sec. VI oscillates around the corresponding value of excess power along the exact optimal protocol (20). As N increases, the oscillations decrease in the central part of the protocol.

Mathematically, this can be translated as

$$\langle \dot{W}_{\text{irr}} \rangle = \frac{d\lambda}{dt} \left(\left\langle \frac{\partial H}{\partial \lambda} \right\rangle - \frac{\partial F}{\partial \lambda} \right), \quad (52)$$

where $\partial F / \partial \lambda$ denotes the derivative of the free energy. Both $\langle \partial_\lambda H \rangle = \langle x^2 \rangle / 2$ and $\partial_\lambda F$ must be evaluated along the protocol $\lambda(t)$.

Reference [26] shows that the functional (34) for a single control parameter predicts a constant excess power along the optimal protocol. Although this reveals an important feature of the physics of slowly varying optimal protocols, it remains to be verified whether this also applies to other nonequilibrium regimes. Figure 9 compares the excess power [Eq. (52)] obtained from the numerical simulations of Eq. (1) using the optimal protocol (46) and the exact optimal protocol (20) for $\tau_R / \tau < 1$. The initial variation is expected since in the exact dynamics there is no driving exactly before the process begins.

Figures 10 and 11 compare the numerical calculations of the excess power using the approximate optimal protocol that minimizes Eq. (47) in the regime of fast but weak processes. The exact optimal protocol leads once more to a constant value, whereas the approximate one yields oscillations around this value. As N increases, our results point to a decrease of the oscillations taking place in the central part of the protocol, becoming, however, more salient at the extremities. It remains to be verified whether the results of this section are a consequence of the quadratic confinement of the Brownian motion [23,39,68].

VIII. CONCLUSION

Using an overdamped driven Brownian particle as a benchmark, we compared the performance of two classes of

approximate optimal protocols to the exact optimal (analytic) solution, performing numerical simulations with realistic parameters and presenting it in units and scales relevant to current experiments. Generally, the approximate protocols have excellent performances in the regions where they were designed. However, one of our main results is how effectively good the performance can be even far outside the region where the approximation is expected to be valid. Hence, our results go beyond determining the range of validity of the perturbative approaches. Moreover, due to the difficulties controlling the approximations involved in the linear-response descriptions (see Refs. [36,69]), this numerical determination is a welcome achievement in itself.

Our analysis shows a clear advantage of the perturbative formulation in describing the optimal energetic cost far from equilibrium compared to the geometric approach. In particular, we verified that the performance of protocols derived from the geometric methods decreases considerably as the duration of the process becomes comparable to the relaxation time.

Despite underperforming in the region of slowly varying processes, the linear response method for fast but weak optimal protocols performs exceptionally well in other regions. Furthermore, these approximate optimal protocols can be more easily implemented experimentally due to their smooth character. At first this might be taken as a weak claim since the exact optimal protocol could also be smoothed out. However, due to the singular character of the jumps, it is not obvious that simple smooth versions of them would also perform well. Therefore, we consider this a nontrivial result obtained from the linear-response approach of Sec. VI. Indeed, as shown in Ref. [70], we could argue that the smoothing we get here is not arbitrary, but one obtained from an optimization procedure that captures certain symmetries.

In this case, the excess power oscillates and can even show negative values. This suggests that nonmonotonic driving might do a good job far from equilibrium as long as it combines oscillations with a steady change, as shown in Figs. 5 and 11. However, we emphasize that the oscillations are not arbitrary but guided by the optimization of Eq. (47) [70], and therefore it is worth investigating further. This fact supports the claim that the perturbative approaches may increase our physical understanding of optimal nonequilibrium processes compared to purely numerical optimization methods.

ACKNOWLEDGMENTS

L.P.K. acknowledges financial support by CNPq (Centro Nacional de Desenvolvimento Científico e Tecnológico), Grant No. 131013/2020-3. M.V.S.B. and S.R.M. acknowledge financial support by FAPESP (Fundação de Amparo à Pesquisa do Estado de São Paulo), Grants No. 2020/02170-4 and No. 2019/27471-0.

- [1] S. Chu, Cold atoms and quantum control, *Nature (London)* **416**, 206 (2002).
 [2] L. M. K. Vandersypen and I. L. Chuang, NMR techniques for quantum control and computation, *Rev. Mod. Phys.* **76**, 1037 (2005).

- [3] C. P. Koch, M. Lemeshko, and D. Sugny, Quantum control of molecular rotation, *Rev. Mod. Phys.* **91**, 035005 (2019).
 [4] A. Kumar and J. Bechhoefer, Exponentially faster cooling in a colloidal system, *Nature (London)* **584**, 64 (2020).

- [5] S. Iram, E. Dolson, J. Chiel, J. Pelesko, N. Krishnan, Ö. Güngör, K. Kuznets-Speck, S. Deffner, E. Ilker, J. G. Scott, and M. Hinczewski, Controlling the speed and trajectory of evolution with counterdiabatic driving, *Nat. Phys.* **17**, 135 (2021).
- [6] S. Deffner and M. V. S. Bonança, Thermodynamic control—An old paradigm with new applications, *Europhys. Lett.* **131**, 20001 (2020).
- [7] T. Schmiedl and U. Seifert, Optimal Finite-Time Processes in Stochastic Thermodynamics, *Phys. Rev. Lett.* **98**, 108301 (2007).
- [8] A. Gomez-Marin, T. Schmiedl, and U. Seifert, Optimal protocols for minimal work processes in underdamped stochastic thermodynamics, *J. Chem. Phys.* **129**, 024114 (2008).
- [9] V. Blickle, T. Speck, L. Helden, U. Seifert, and C. Bechinger, Thermodynamics of a Colloidal Particle in a Time-Dependent Nonharmonic Potential, *Phys. Rev. Lett.* **96**, 070603 (2006).
- [10] P. Jop, A. Petrosyan, and S. Ciliberto, Work and dissipation fluctuations near the stochastic resonance of a colloidal particle, *Europhys. Lett.* **81**, 50005 (2008).
- [11] A. Imparato, P. Jop, A. Petrosyan, and S. Ciliberto, Probability density functions of work and heat near the stochastic resonance of a colloidal particle, *J. Stat. Mech.* (2008) P10017.
- [12] V. Blickle and C. Bechinger, Realization of a micrometre-sized stochastic heat engine, *Nat. Phys.* **8**, 143 (2012).
- [13] K. Proesmans, Y. Dreher, M. Gavrilov, J. Bechhoefer, and C. Van den Broeck, Brownian Duet: A Novel Tale on Thermodynamic Efficiency, *Phys. Rev. X* **6**, 041010 (2016).
- [14] I. A. Martínez, É. Roldán, L. Dinis, and R. A. Rica, Colloidal heat engines: A review, *Soft Matter* **13**, 22 (2017).
- [15] S. Toyabe, T. Sagawa, M. Ueda, E. Muneyuki, and M. Sano, Experimental demonstration of information-to-energy conversion and validation of the generalized Jarzynski equality, *Nat. Phys.* **6**, 988 (2010).
- [16] É. Roldán, I. A. Martínez, J. M. R. Parrondo, and D. Petrov, Universal features in the energetics of symmetry breaking, *Nat. Phys.* **10**, 457 (2014).
- [17] A. Bérut, A. Arakelyan, A. Petrosyan, S. Ciliberto, R. Dillenschneider, and E. Lutz, Experimental verification of Landauer's principle linking information to thermodynamics, *Nature (London)* **483**, 187 (2012).
- [18] Y. Jun, M. Gavrilov, and J. Bechhoefer, High-Precision Test of Landauer's Principle in a Feedback Trap, *Phys. Rev. Lett.* **113**, 190601 (2014).
- [19] M. Gavrilov and J. Bechhoefer, Erasure Without Work in an Asymmetric Double-Well Potential, *Phys. Rev. Lett.* **117**, 200601 (2016).
- [20] S. Blaber, M. D. Louwerse, and D. A. Sivak, Steps minimize dissipation in rapidly driven stochastic systems, *Phys. Rev. E* **104**, L022101 (2021).
- [21] H. Then and A. Engel, Computing the optimal protocol for finite-time processes in stochastic thermodynamics, *Phys. Rev. E* **77**, 041105 (2008).
- [22] P. Geiger and C. Dellago, Optimum protocol for fast-switching free-energy calculations, *Phys. Rev. E* **81**, 021127 (2010).
- [23] E. Aurell, C. Mejía-Monasterio, and P. Muratore-Ginanneschi, Optimal Protocols and Optimal Transport in Stochastic Thermodynamics, *Phys. Rev. Lett.* **106**, 250601 (2011).
- [24] E. Aurell, C. Mejía-Monasterio, and P. Muratore-Ginanneschi, Boundary layers in stochastic thermodynamics, *Phys. Rev. E* **85**, 020103(R) (2012).
- [25] C. A. Plata, D. Guéry-Odelin, E. Trizac, and A. Prados, Optimal work in a harmonic trap with bounded stiffness, *Phys. Rev. E* **99**, 012140 (2019).
- [26] D. A. Sivak and G. E. Crooks, Thermodynamic Metric and Optimal Paths, *Phys. Rev. Lett.* **108**, 190602 (2012).
- [27] P. R. Zulkowski, D. A. Sivak, G. E. Crooks, and M. R. DeWeese, Geometry of thermodynamic control, *Phys. Rev. E* **86**, 041148 (2012).
- [28] M. V. S. Bonança and S. Deffner, Optimal driving of isothermal processes close to equilibrium, *J. Chem. Phys.* **140**, 244119 (2014).
- [29] P. R. Zulkowski and M. R. DeWeese, Optimal control of overdamped systems, *Phys. Rev. E* **92**, 032117 (2015).
- [30] P. R. Zulkowski and M. R. DeWeese, Optimal protocols for slowly driven quantum systems, *Phys. Rev. E* **92**, 032113 (2015).
- [31] D. A. Sivak and G. E. Crooks, Thermodynamic geometry of minimum-dissipation driven barrier crossing, *Phys. Rev. E* **94**, 052106 (2016).
- [32] G. M. Rotskoff and G. E. Crooks, Optimal control in nonequilibrium systems: Dynamic Riemannian geometry of the Ising model, *Phys. Rev. E* **92**, 060102(R) (2015).
- [33] G. M. Rotskoff, G. E. Crooks, and E. Vanden-Eijnden, Geometric approach to optimal nonequilibrium control: Minimizing dissipation in nanomagnetic spin systems, *Phys. Rev. E* **95**, 012148 (2017).
- [34] J. N. E. Lucero, A. Mehdizadeh, and D. A. Sivak, Optimal control of rotary motors, *Phys. Rev. E* **99**, 012119 (2019).
- [35] M. Scandi and M. Perarnau-Llobet, Thermodynamic length in open quantum systems, *Quantum* **3**, 197 (2019).
- [36] S. Blaber and D. A. Sivak, Skewed thermodynamic geometry and optimal free energy estimation, *J. Chem. Phys.* **153**, 244119 (2020).
- [37] P. Abiuso and M. Perarnau-Llobet, Optimal Cycles for Low-Dissipation Heat Engines, *Phys. Rev. Lett.* **124**, 110606 (2020).
- [38] M. D. Louwerse and D. A. Sivak, Multidimensional minimum-work control of a 2D Ising model, *J. Chem. Phys.* **156**, 194108 (2022).
- [39] S. Blaber and D. A. Sivak, Efficient two-dimensional control of barrier crossing, *Europhys. Lett.* **139**, 17001 (2022).
- [40] N. S. Wadia, R. V. Zarcone, and M. R. DeWeese, Solution to the Fokker-Planck equation for slowly driven Brownian motion: Emergent geometry and a formula for the corresponding thermodynamic metric, *Phys. Rev. E* **105**, 034130 (2022).
- [41] A. G. Frim and M. R. DeWeese, Geometric Bound on the Efficiency of Irreversible Thermodynamic Cycles, *Phys. Rev. Lett.* **128**, 230601 (2022).
- [42] A. G. Frim and M. R. DeWeese, Optimal finite-time Brownian Carnot engine, *Phys. Rev. E* **105**, L052103 (2022).
- [43] M. de Koning and A. Antonelli, Adiabatic switching applied to realistic crystalline solids: Vacancy-formation free energy in copper, *Phys. Rev. B* **55**, 735 (1997).
- [44] P. Salamon and R. S. Berry, Thermodynamic Length and Dissipated Availability, *Phys. Rev. Lett.* **51**, 1127 (1983).
- [45] G. Ruppeiner, Riemannian geometry in thermodynamic fluctuation theory, *Rev. Mod. Phys.* **67**, 605 (1995).
- [46] G. E. Crooks, Measuring the Thermodynamic Length, *Phys. Rev. Lett.* **99**, 100602 (2007).
- [47] M. V. S. Bonança and S. Deffner, Minimal dissipation in processes far from equilibrium, *Phys. Rev. E* **98**, 042103 (2018).

- [48] O. M. Maragò, P. H. Jones, P. G. Gucciardi, G. Volpe, and A. C. Ferrari, Optical trapping and manipulation of nanostructures, *Nat. Nanotechnol.* **8**, 807 (2013).
- [49] P. H. Jones, O. M. Maragò, and G. Volpe, *Optical Tweezers: Principles and Applications* (Cambridge University Press, Cambridge, 2015).
- [50] J. Gieseler, J. R. Gomez-Solano, A. Magazzù, I. P. Castillo, L. P. García, M. Gironella-Torrent, X. Viader-Godoy, F. Ritort, G. Pesce, A. V. Arzola, K. Volke-Sepúlveda, and G. Volpe, Optical tweezers—From calibration to applications: A tutorial, *Adv. Opt. Photon.* **13**, 74 (2021).
- [51] S. K. Otani, T. T. Martins, S. R. Muniz, P. C. de Sousa Filho, F. A. Sigoli, and R. A. Nome, Spectroscopic characterization of rare events in colloidal particle stochastic thermodynamics, *Front. Chem.* **10**, 879524 (2022).
- [52] T. T. Martins and S. R. Muniz, Dynamically controlled double-well optical potential for colloidal particles, in *2021 SBFoton International Optics and Photonics Conference (SBFoton IOPC)* (IEEE, 2021), pp. 1–4, doi:10.1109/SBFotonIOPC50774.2021.9461866.
- [53] G. H. Oliveira, M. T. Galante, T. T. Martins, L. F. L. S. dos Santos, F. Ely, C. Longo, R. V. Gonçalves, S. R. Muniz, and R. A. Nome, Real time single TiO₂ nanoparticle monitoring of the photodegradation of methylene blue, *Solar Energy* **190**, 239 (2019).
- [54] G. Volpe and G. Volpe, Simulation of a Brownian particle in an optical trap, *Am. J. Phys.* **81**, 224 (2013).
- [55] K. Sekimoto, Langevin equation and thermodynamics, *Prog. Theor. Phys. Suppl.* **130**, 17 (1998).
- [56] T. Schmiedl and U. Seifert, Efficiency of molecular motors at maximum power, *Europhys. Lett.* **83**, 30005 (2008).
- [57] I. Martínez, É. Roldán, L. Dinis, D. Petrov, J. M. R. Parrondo, and R. A. Rica, Brownian Carnot engine, *Nat. Phys.* **12**, 67 (2016).
- [58] H. Risken, *The Fokker-Planck Equation* (Springer-Verlag, New York, 1996).
- [59] L. E. Reichl, *A Modern Course in Statistical Physics*, 2nd ed. (Wiley, New York, 1998).
- [60] H. B. Callen, *Thermodynamics and an introduction to thermostatistics* (Wiley, New York, 1998).
- [61] C. A. Plata, D. Guéry-Odelin, E. Trizac, and A. Prados, Finite-time adiabatic processes: Derivation and speed limit, *Phys. Rev. E* **101**, 032129 (2020).
- [62] L.-W. Tsao, S.-Y. Sheu, and C.-Y. Mou, Absolute entropy of simple point charge model water by adiabatic switching processes, *J. Chem. Phys.* **101**, 2302 (1994).
- [63] R. Kubo, M. Toda, and N. Hashitsume, *Statistical Physics II: Nonequilibrium Statistical Mechanics*, 2nd ed., Solid State Sciences Vol. 31 (Springer, Berlin, 2012).
- [64] For protocols with multiple control parameters, this term is part of the so-called friction tensor [26,71].
- [65] M. de Koning, Optimizing the driving function for nonequilibrium free-energy calculations in the linear regime: A variational approach, *J. Chem. Phys.* **122**, 104106 (2005).
- [66] T. V. Acconcia and M. V. S. Bonança, Degenerate optimal paths in thermally isolated systems, *Phys. Rev. E* **91**, 042141 (2015).
- [67] A. Weiße, G. Wellein, A. Alvermann, and H. Fehske, The kernel polynomial method, *Rev. Mod. Phys.* **78**, 275 (2006).
- [68] S. Blaber and D. A. Sivak, Optimal control with a strong harmonic trap, *Phys. Rev. E* **106**, L022103 (2022).
- [69] P. Nazé and M. V. S. Bonança, Series expansion of the excess work using nonlinear response theory, *J. Stat. Phys.* **186**, 23 (2022).
- [70] P. Nazé, S. Deffner, and M. V. S. Bonança, Optimal finite-time processes in weakly driven overdamped Brownian motion, *J. Phys. Commun.* **6**, 083001 (2022).
- [71] J. G. Kirkwood, The statistical mechanical theory of transport processes I. General theory, *J. Chem. Phys.* **14**, 180 (1946).